Received: 1 February 2022 | Revised: 23 December 2022 | Accepted: 1 February 2023

DOI: 10.1002/acs.3566

RESEARCH ARTICLE

WILEY

Wind turbine emulator control improvement using nonlinear PI controller for wind energy conversion system: Design and real-time implementation

Abdeldjebar Hazzab[1,2] | **Hicham Gouabi**[1] | **Mohamed Habbab**[1] | **Miloud Rezkallah**[2,3] | **Hussein Ibrahim**[3] | **Ambrish Chandra**[2]

[1]Laboratoire de Recherche: Commande, Analyse et Optimisation des Systèmes Electro-Energétiques (CAOSEE), Université Tahri Mohamed, Bechar, Algeria

[2]École de Technologie Supérieure, Montréal, Québec, Canada

[3]Centre de Recherche de Gestion énergétique Intelligente des Systèmes Industriels et dans les Bâtiments (CR2ie)., Cégep de Sept-Îles, Sept-Îles, Québec, Canada

Correspondence
Abdeldjebar Hazzab, École de Technologie Supérieure, Montréal, Québec, Canada.
Email: hazzab.abdeldjebar@etsmtl.ca and abdeldjebar.hazzab@gmail.com

Summary

Wind turbine emulators (WTE) have become a necessity for testing, developing, and improving design and control strategies in the renewable energy domain. The aim of this paper is to realize an experimental standalone wind energy conversion system emulator (WECSE) with improved torque and current control strategy using a nonlinear PI controller. The prototype was developed with a separately excited DC motor to simulate the wind turbine by providing the required speed and torque for power generation using a directly driven wound-rotor synchronous generator and a power conversion system controlled by a modified drift-free Perturb and Observe (P&O) Maximum Power Point Tracking algorithm (MPPT). The DC motor torque is controlled by an nonlinear PI controller regulator for an estimated current reference through a chopper driven by a dSPACE control board where the MATLAB/Simulink platform is used for wind turbine simulation. The proposed method was validated by experimental tests for different wind speeds and was compared with the conventional method. The experimental results have demonstrated that the control, emulation, and MPPT performances of the proposed method are significantly better.

KEYWORDS

emulator, MPPT, nonlinear PI controller, perturb and observe, wind turbine

1 | INTRODUCTION

Recently, in order to meet the growing demand for electricity, together with the need to minimize environmental problems arising from the levels of carbon dioxide emission, a contributor to global warming and climate change, initiatives in the search for the development of new technologies aimed at the production of electric energy through renewable sources had a great evolution in the last years.[1] Among the alternative sources for energy generation, wind energy is considered one of the most important and promising, mainly due to its economic viability, low cost/benefit ratio of exploration, for presenting a rapid technological development and, mainly, due to governmental incentives, carried out in recent years.[1-3]

With more than 93 GW of installed wind power and a growth of 53%, last year was the global wind industry's best year ever, bringing global cumulative wind power capacity up to 743 GW.[4]

This rapid development of wind power systems has led to a significant increase in problems related to the use of wind generation as a form of distributed generation operating in grid isolated or connected. These problems have motivated the scientific community to research and propose different control topologies, generating considerable research carried out in recent years. During the initial steps in the development of wind power systems, it is convenient to carry out trials and tests of control strategies in a laboratory environment. As a wind turbine (WT) has a large dimension and a high cost, it is not economically viable to use it for research development. The Wind Turbine Emulator (WTE) reproduces the static and dynamic behaviors of a real-WT system in the laboratory even though the weather conditions are often intermittent or nonexistent. Thus, engineers must be taught how to operate and regulate Wind Energy Conversion Systems (WECS) to generate qualified staff for the industry. As a result, developing controlled test platforms that can realize the emulation of large-inertia WTs utilizing small-inertia electric machines even in the absence of wind is crucial in experiments. As a result, WTEs are the most cost-effective solution for this, in which its correct representation becomes essential for the technological development of the area.[5] In addition, the WTE is an important tool for the analysis of impacts caused by the connection of wind farms in the energy distribution network. Thus, the implementation of a WTE is convenient for the study of energy quality improvement, a concept that has been widely studied over the years.[6,7]

WECS operation speed can be fixed or variable. The latter is a better choice than fixed speed because of its better control performance, lower acoustic noise and mechanical stresses, and higher efficiency and power quality, making it the most suitable for wind power applications.[8-10] Variable speed WECS make use of a variety of generator types, such as doubly fed and squirrel-cage induction generators,[11-15] permanent-magnet, and wound-rotor synchronous generators (WRSG).[16-19] The use of the gearless permanent magnet synchronous generator for WECS has become more important due to its low losses, minimal cost of maintenance, high efficiency, and self-excitation.[20] The DC motor drive is frequently used for WTE,[21] compared to the permanent magnet synchronous motor drive,[22] or squirrel cage induction motor drive,[23] because of the simplicity of its implementation in the control.

Generally, the emulators are controlled in a closed loop that adjusts the motor variables to be as similar as possible to the WT curves. In fact, the speed and the current or torque of the motor are recovered through sensors, and after that, using a processor or computer, reference signals will be generated on a digital platform across analog digital converter (ADC) converters.[24,25]

The nonlinear PI controller (NLPI) is a hybridization between the conventional PI (CPI) control and the modern model-based approaches that allow for a double advantage: easy applicability, as well as better performance and robustness of control. Most of the disturbances and modeling uncertainties in the system control are taken into consideration by the NLPI controller foundation. Therefore, the design of the control loop requires only a very coarse process model. These advantages make the NLPI controller a favorable choice for practitioners due to its good robustness against process variations.[26,27]

This work presents the development of an experimental test bench of WTE, having a primary DC motor, coupled directly to a WRSG, by the integration of a NLPI controller to control the torque by controlling the DC motor current through a chopper driven by a dSPACE (DS1104), to emulate a variable speed WECS where the WT torque is simulated in MATLAB/Simulink and applied to the WTE motor. The real-time application of the NLPI in the control loop of the WTE sytems presents the originality of this work. The rest of the paper is structured as follows: The second section explains the WT model. The third section describes the structure of the WTE used in this paper. Experimental results are shown and discussed in the fourth section, while fifth section is the conclusion of this paper.

2 | WT MODEL

The generator coupled to the WT converts the linear wind speed into an angular wind speed when the blades turn. This movement creates electrical energy from wind kinetic energy.

The following equation expresses the mechanical power captured by the WT:[17]

$$P_m = \frac{1}{2}\rho A v^3 C_p(\lambda, \beta), \tag{1}$$

where ρ is density of air (kg/m^3), $A = \pi R^2$ is area that is swept by the blades of the turbine (m^2), R is the ray of the blade (m), $C_p(\lambda, \beta)$ is power coefficient, and v is wind speed (m/s).

Equations (2) and (3) present the expression of:[18]

$$C_p(\lambda,\beta) = 0.5176\left(\frac{116}{\lambda_i} - 0.4\beta - 5\right)e^{-21/\lambda_i} + 0.0068\lambda_i, \tag{2}$$

$$\frac{1}{\lambda_i} = \frac{1}{\lambda + 0.08\beta} - \frac{0.035}{\beta^3 + 1}, \tag{3}$$

where β is the blade pitch angle (deg) and λ is mathematically expressed as following:[18]

$$\lambda = \frac{\omega_r R}{v}, \tag{4}$$

where ω_r is the angular speed of the blades (rad/s).

The WT's optimum captured power can be expressed from (1) and (4) as follows:[28]

$$P_{m_{\text{opt}}} = \frac{0.5\pi\rho C_{p_{max}} R^5}{\lambda_{\text{opt}}^3}\omega_r^3 = K_{\text{opt}}\omega_r^3. \tag{5}$$

$C_{p_{\max}}$ is the maximum value $C_p(\lambda,\beta)$ at a location known as the lambda optimum (λ_{opt}). The turbine obtains the maximum power from the wind by following the $C_{p_{\max}}$ curve.[17]

3 | WTE STRUCTURE

The principle of the emulation is to generate an aerodynamic torque to directly drive the WECS.

From (1), and since mechanical torque can be defined as:[29]

$$T_m = \frac{P_m}{\omega_r}. \tag{6}$$

The generated aerodynamic torque expression can be given:

$$T_m = \frac{\rho A v^3 C_p(\lambda,\beta)}{2\omega_r}. \tag{7}$$

The reference current for the DC motor control can be expressed as follows:[30]

$$i_{\text{dcm}}^* = \frac{T_m}{I_{ex}K_{\text{dcm}}}. \tag{8}$$

Where I_{ex} is the excitation current and K_{dcm} is the torque constant.

From (7) and (8), in a constant pitch angle, the DC motor reference current depends on wind speed:

$$i_{\text{dcm}}^* = \frac{\rho A C_p(\lambda,\beta)}{2I_{\text{ex}}K_{\text{dcm}}\omega_r}v^3. \tag{9}$$

The experimental prototype for the WTE is illustrated in Figure 1 and Figure 2 presents the experimental setup of the developed WTE.

The main elements of the test bench (Table 1) are an insulated gate bipolar transistor (IGBT)-based chopper, powered by a fixed voltage power supply, to supply a separately excited DC motor with a constant voltage of excitation. The WTE drives the WRSG directly, which is coupled to the three-phase diode rectifier, and the resultant rectified output is connected to a DC-to-DC buck converter through a DC link capacitor. For the control strategy of the DC motor, the angular speed of the rotor is sensed using a speed incremental encoder connected to the dSPACE incremental encoder interface,

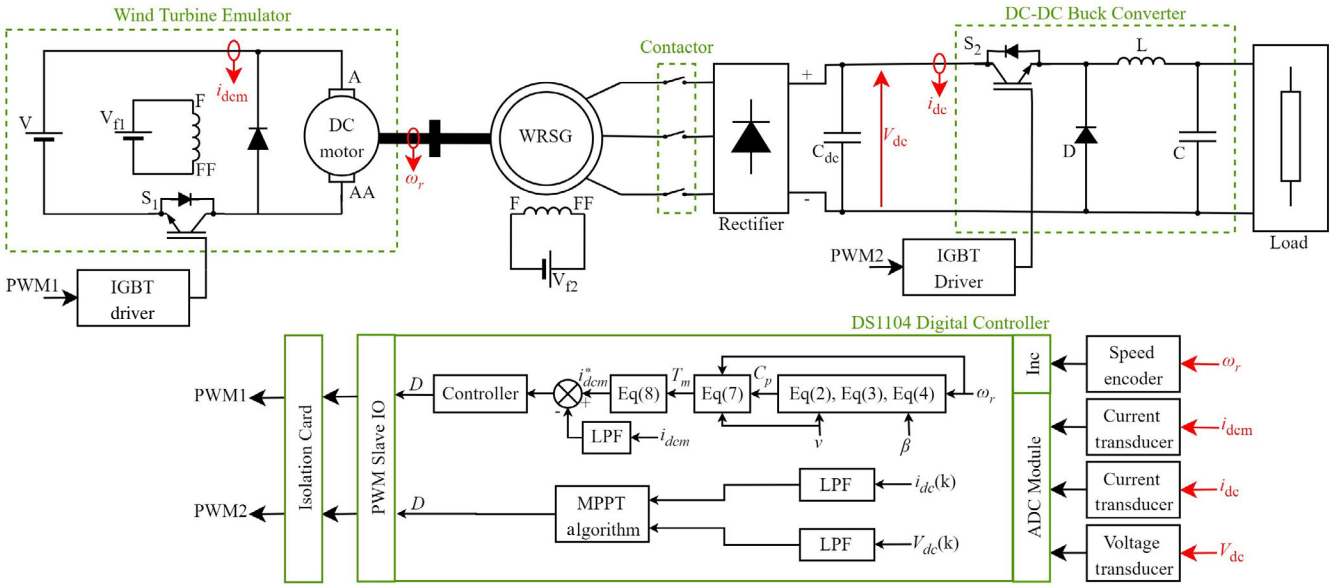

FIGURE 1 Circuit diagram of wind turbine emulators with digital controller.

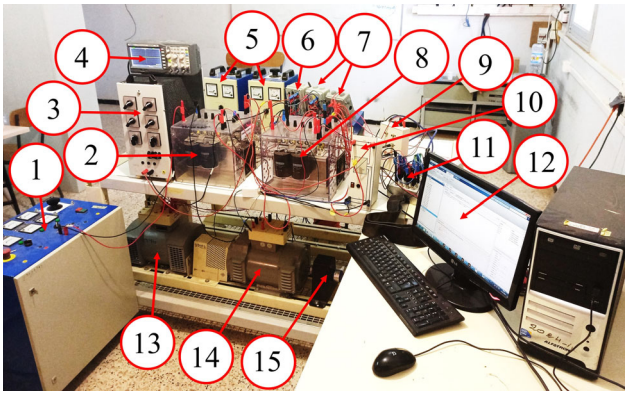

FIGURE 2 Experimental setup of the developed wind turbine emulator.

and the DC current is sensed by a Hall effect LA 25-NP - Lem - Current Sensor and, the signal is transmitted to the ADC module of the dSPACE before being filtered by a digital low pass filter.

The power coefficient $C_p(\lambda, \beta)$ is calculated based on the measured rotor angular speed (ω_r), constant blade pitch angle (β), and variable wind speed (v) by using Equations (2), (3), and (4). After that, the WT mechanical torque (T_m) is calculated using Equation (7).

The parameters of the WT are listed in Table 2. The DC motor reference current (i^*_{dcm}) is estimated from T_m using Equation (8). Table 3 shows the different parameters of the DC motor.

The duty cycle (D) is generated by the controller after comparing the DC motor reference current and the measured one; two control methods were applied and compared, the CPI and the NLPI one.

The mathematical expression of the CPI controller is given by:[22]

$$D = K_p e + K_i \int_t^{t_0} e dt, \tag{10}$$

where e is the error between i^*_{dcm} and i_{dcm}, and K_p and K_i are the proportional and integral gains, respectively.

TABLE 1 List of the main elements of the test bench.

1	Source for the chopper
2	Chopper
3	Resistive load
4	Cathode Ray Oscilloscope
5	DC excitation sources for the DC motor and generator
6	Current transducer
7	Voltage transducer
8	Rectifier + DC-DC buck converter
9	Isolation card
10	Power supply ±15 V of transducers and IGBT drivers
11	dSpace DS1104
12	Host computer
13	Wound-rotor synchronous generator (WECS)
14	DC motor
15	Speed incremental encoder

TABLE 2 Wind turbine parameters.

Parameter	Value
Air density (kg/m^3)	1.225
Radius of the blades (m)	0.95
Blades pitch angle (deg)	7

TABLE 3 DC motor nominal values.

Power (kW)	1.5
Voltage (V)	220
Field excitation current (A)	0.32
Torque constant (Nm/A^2)	2.7
Speed (rpm)	1500

In this work, the NLPI controller proposed by Han (1994)[31] is used to generate the duty cycle (D) as follow:

$$D = K_p \mathrm{fal}(e, \alpha_p, \delta_p) + K_i \int_t^{t_0} \mathrm{fal}(edt, \alpha_p, \delta_p). \tag{11}$$

With $fal(x, \alpha_p, \delta_p)$ is a nonlinear function expressed as:

$$\mathrm{fal}(x, \alpha_p, \delta_p) = \begin{cases} |x|^{\alpha} \mathrm{sign}(x), & |x| > \delta \\ \frac{x}{\delta^{1-\alpha}}, & |x| \leqslant \delta \end{cases}, \tag{12}$$

where α and δ are constants.

The idea of the NLPI controller is to use a nonlinear combination of e and $\int_t^{t_0} edt$ instead of the linear one.

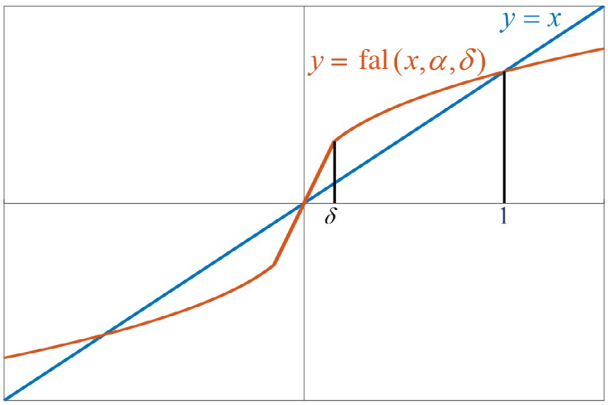

FIGURE 3 Impact of the nonlinear function fal(x, α_p, δ_p).

TABLE 4 PI and nonlinear PI controllers' parameters.

K_p	K_i	α_p	δ_p	α_i	δ_i
0.05	0.15	0.98	0.5	0.75	0.5

Figure 3 shows the impact of the nonlinear function. It can be shown that when $\alpha = 1$ and $\delta = 0$, the controller becomes a conventional linear PI. On the other hand, choosing other values for the gains leads to new and different behaviors of the controller.

fal(x, α_p, δ_p) gives big gains for small x and small gains for high x. Thus, α is conventionally the error weighting and δ selects the linear area in the nonlinear behavior where the controller acts like the linear PI.

The used parameters for the CPI and the NLPI are presented in Table 4.

For the MPPT control of the WECS, dc-link current and voltage are sensed using the Hall Effect LA-25-NP-Lem current sensor and LV-25-P-Lem voltage transducer, respectively. The measurement captured by the dSPACE ADC interface passes through the low pass filter to be used by the MPPT algorithm explained in Section 4 to generate the duty cycle.

The two 20 kHz PWM signals, generated by the dSPACE PWM Slave IO based on the calculated duty cycles, pass through the card of insulation and amplification CD4093BE integrated circuit based, to control the IGBT-based converter.

4 | EXPERIMENTAL RESULTS AND DISCUSSION

All the mathematical development described in the previous sections and the performances of the existing and proposed control schemes for WTE are verified through experiments using the previously described experimental prototype and simulation with MATLAB/Simulink of the WT model detailed in Section 2, under conditions of increasing and decreasing wind speed.

The experimental validation of the WTE will be given by comparing the practical results with the theoretical curves obtained in the MATLAB/Simulink environment. The measurements of input and output power signals of the DC-DC Buck converter and DC motor current signals were recorded by the METRIX digital oscillograph DOX2100B. The values of generated aerodynamic torque, power coefficient, tip speed ratio, and rotor angular speed were made and recorded using the ControlDesk of dSPACE DS1104.

Figure 4 shows the characteristic curve of the WTE power coefficient for different values of the pitch angle β.

The used operation point for the following WTE experimental tests is mentioned with a red color in Figure 4 where the pitch angle is fixed at ($\beta = 7$) and the wind speed varies between 6 and 10 m/s.

The wind speed profile for the increasing and decreasing conditions, is a step from 6 and 10 m/s, and a step from 10 to 8 m/s, respectively.

Figures 5 and 6 show the comparison of i_{dcm} variation when CPI and NLPI controllers are used, for the previously cited conditions of wind speed. It can be observed that the current response when using the NLPI is significantly improved

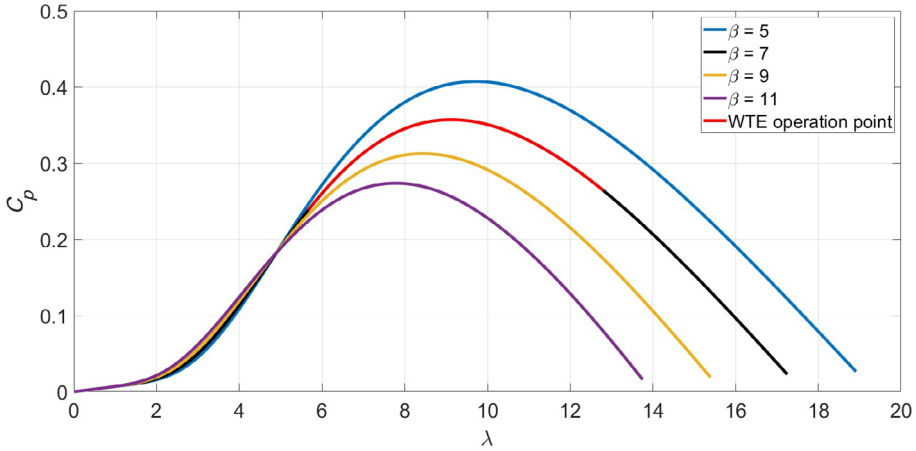

FIGURE 4 Wind turbine characteristic curve $C_p = f(\lambda)$.

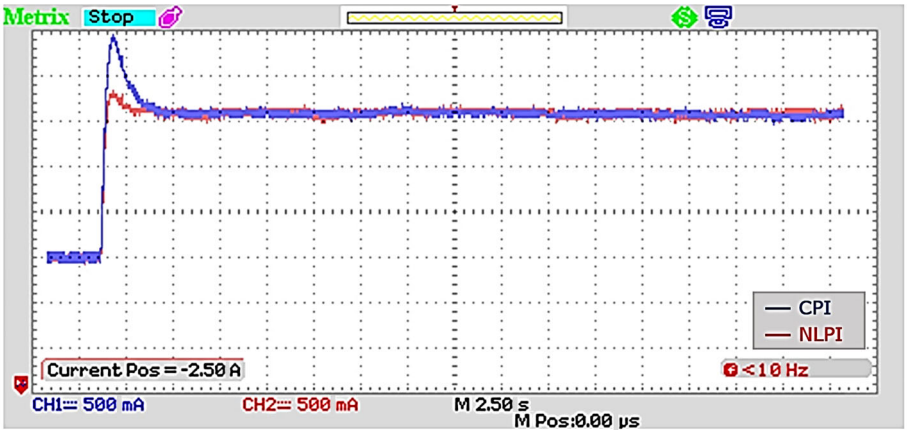

FIGURE 5 Motor current (i_{dcm}) response in the increasing wind speed condition.

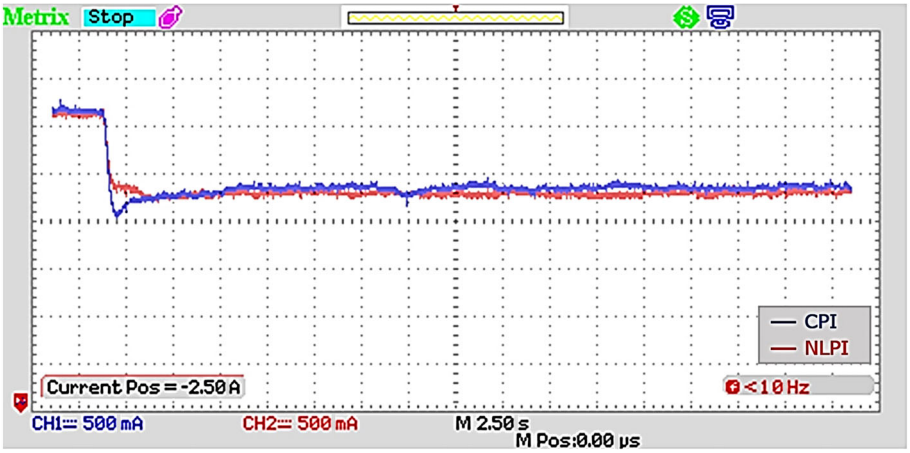

FIGURE 6 Motor current (i_{dcm}) response in the decreasing wind speed condition.

TABLE 5 Motor current response performances for increasing wind speed condition.

Performance	CPI	NLPI
Overshoot (%)	51.27	13.37
Rise time (s)	0.29	0.37
Settling time (s)	2.62	1.28
Current ISE (A^2)	0.75	0.37

Abbreviations: CPI, conventional PI; NLPI, nonlinear PI.

TABLE 6 Motor current response performances for decreasing wind speed condition.

Performance	CPI	NLPI
Overshoot (%)	34.97	5.54
Rise time (s)	0.36	1.96
Settling time (s)	6.45	4.22
Current ISE (A^2)	0.21	0.13

Abbreviations: CPI, conventional PI; NLPI, nonlinear PI.

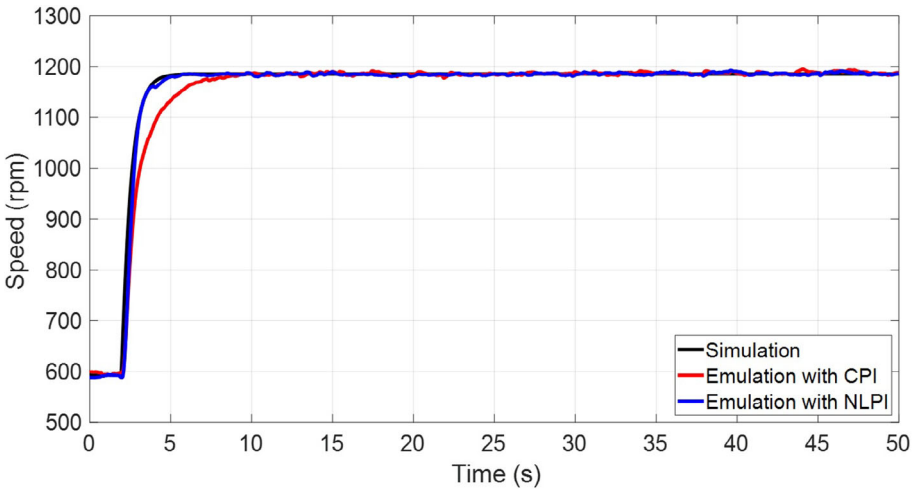

FIGURE 7 Rotor angular speed (ω_r) in the increasing wind speed condition.

with reduced overshoot, undershoot, and settling time. The values of the transient-response specifications presented in Tables 5 and 6 confirm the superiority of NLPI compared with the CPI controller for the practical control system, in particular the maximum overshoot, the maximum undershoot, and the settling time.

For increasing and decreasing wind speed conditions, Figures 7 and 8 show rotor angular speed variations, Figures 9 and 10 present the generated aerodynamic torque (T_m), while the tip speed ratio (λ) is shown in Figures 11 and 12, and the power coefficient (C_p) is presented in Figures 13 and 14. According to these results, the proposed emulator using the NLPI controller perfectly imitates the dynamic and static behavior of the simulated model with a clear improvement in the tracking of the reference model compared to the emulator using the CPI controller, especially in the transient-regime.

The WTE control affects the WECS power performances also. To test the proposed control strategy, a drift-free modified perturb and observe (P&O) MPPT controller, Figure 15, proposed by Mishra et al.[32] is integrated.

Figures 16 and 17 show the DC-DC buck converter input and output powers in the increasing and decreasing wind speed conditions when CPI is used. While in Figures 18 and 19, those power curves are shown when NLPI is implemented.

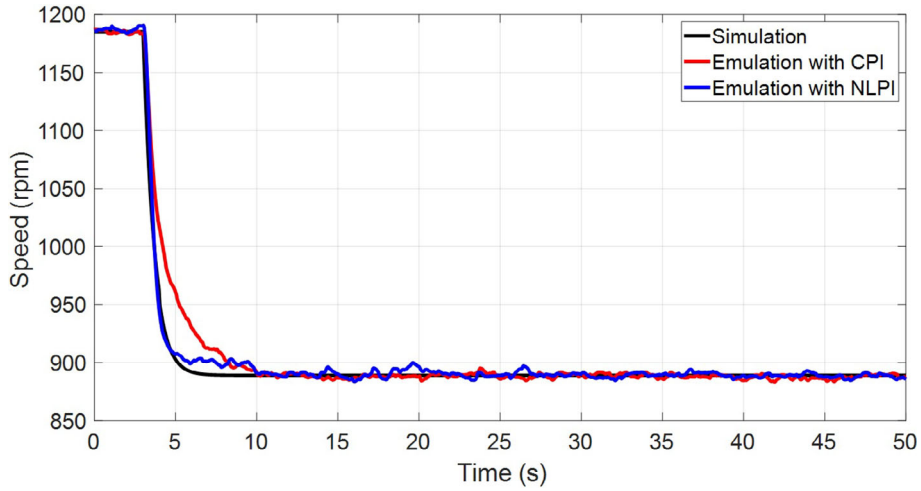

FIGURE 8 Rotor angular speed (ω_r) in the decreasing wind speed condition.

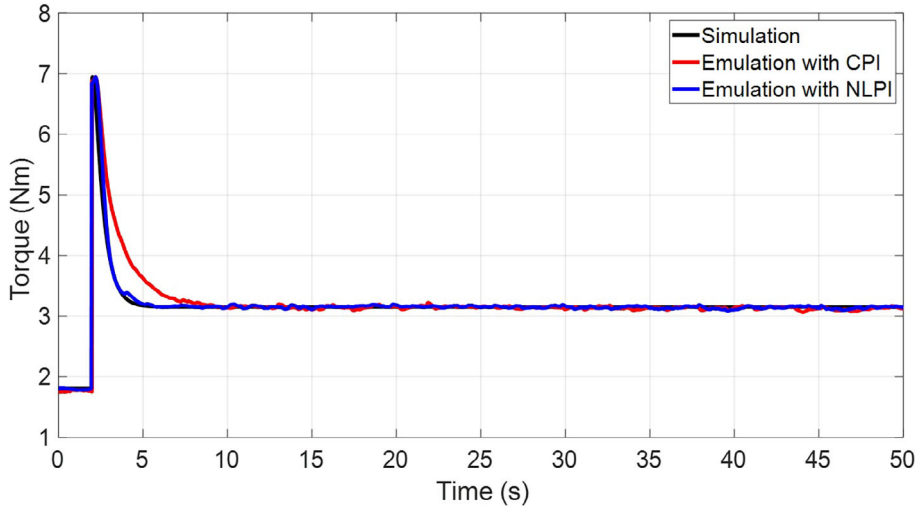

FIGURE 9 Generated aerodynamic torque (T_m) in the increasing wind speed condition.

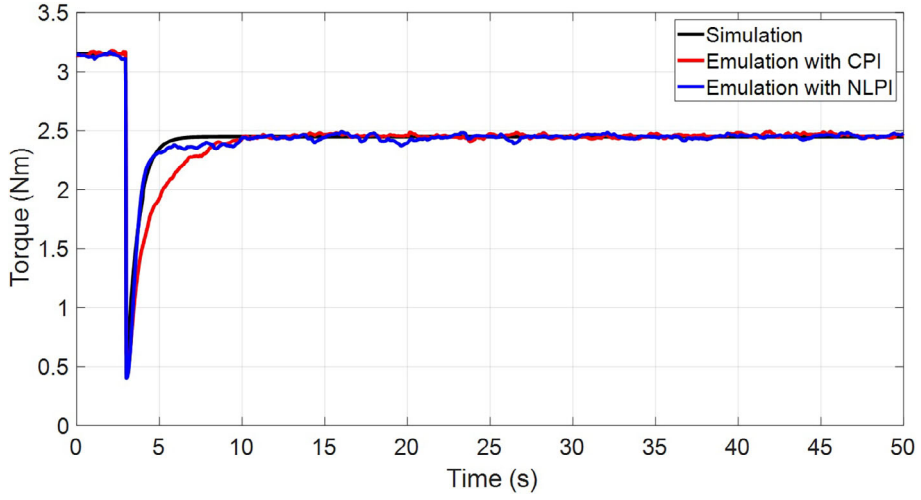

FIGURE 10 Generated aerodynamic torque (T_m) in the decreasing wind speed condition.

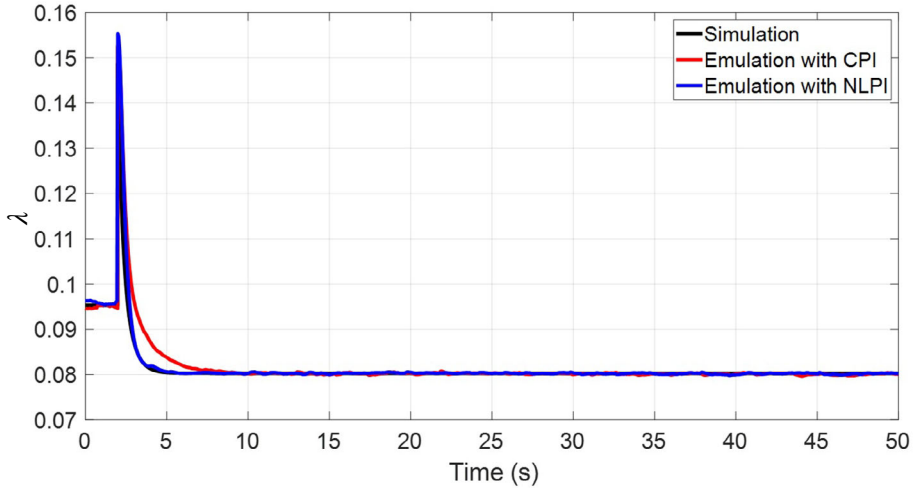

FIGURE 11 Tip speed ratio (λ) in the increasing wind speed condition.

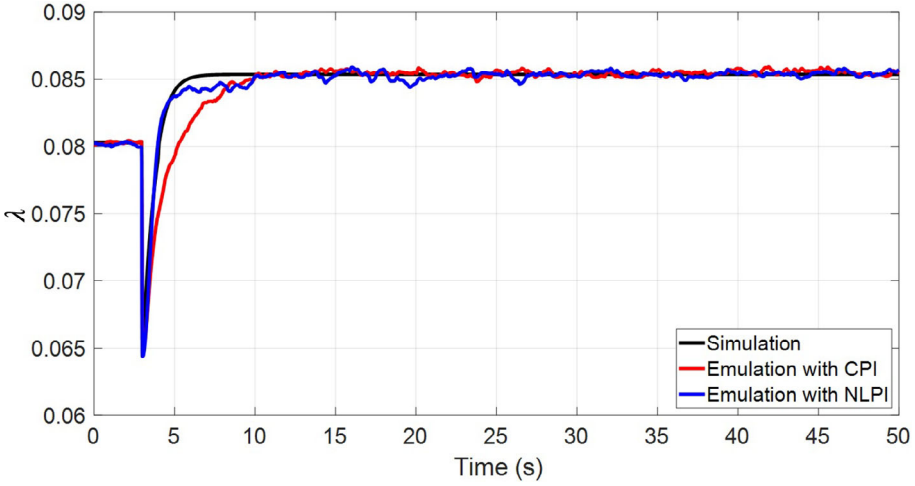

FIGURE 12 Tip speed ratio (λ) in the decreasing wind speed condition.

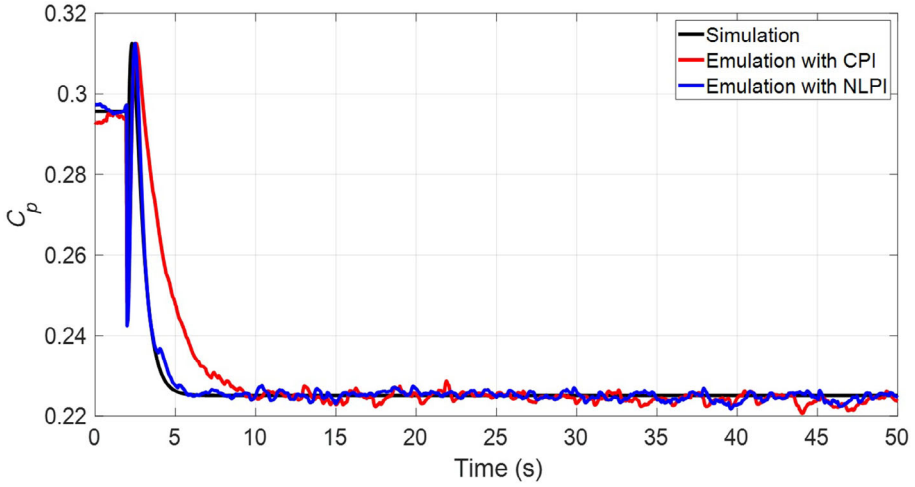

FIGURE 13 Power coefficient (C_p) in the increasing wind speed condition.

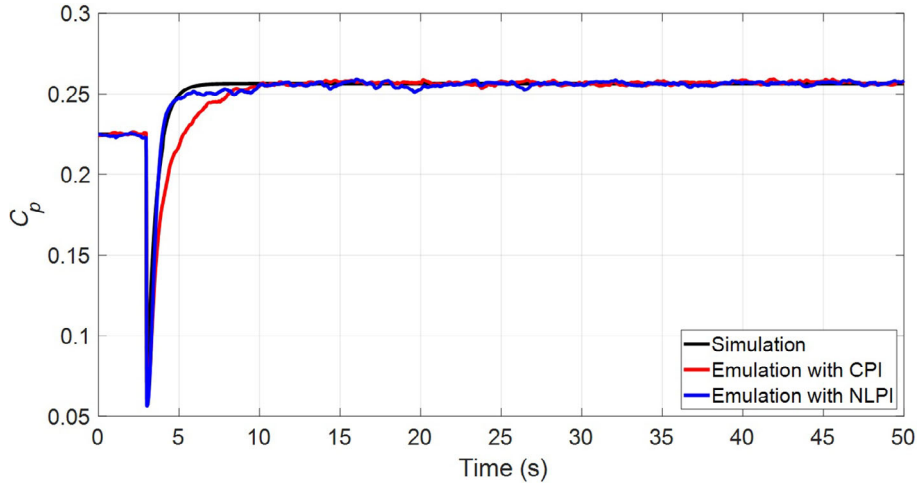

FIGURE 14 Power coefficient (C_p) in the decreasing wind speed condition.

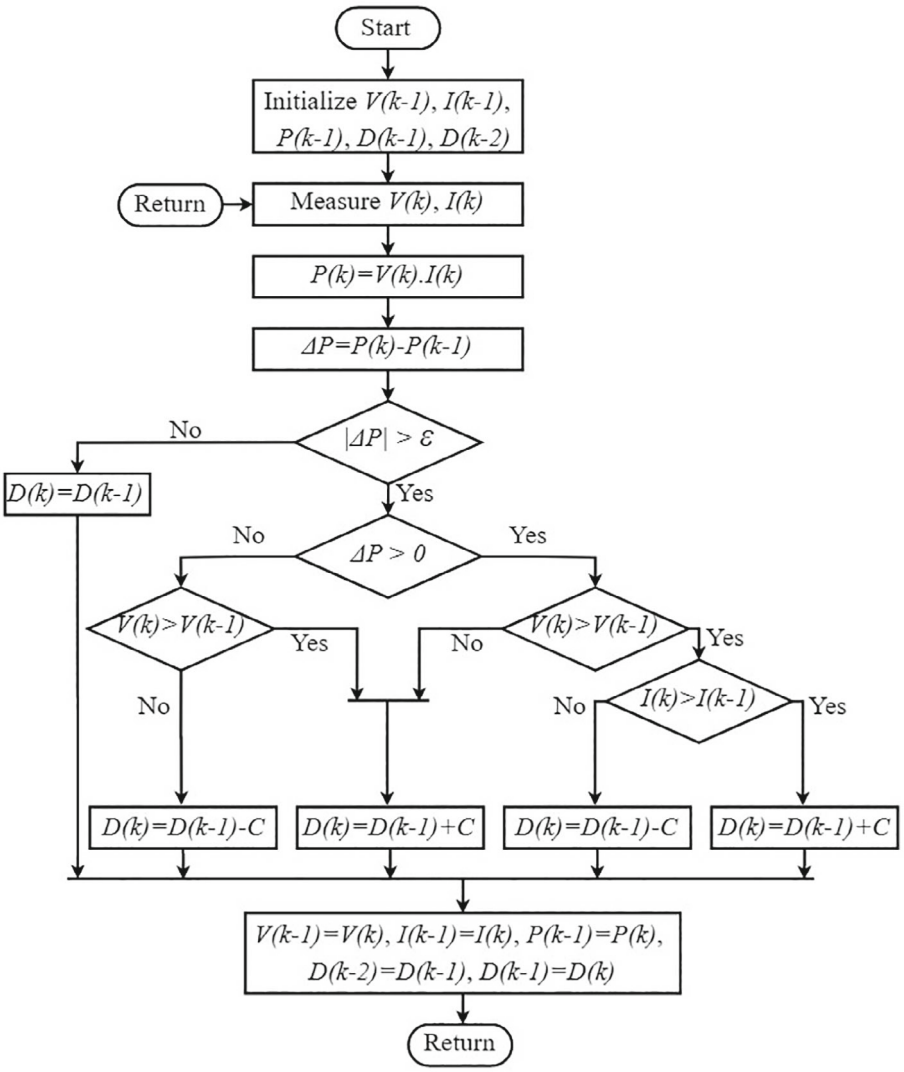

FIGURE 15 Modified perturb and observe maximum power point tracking algorithm.[32]

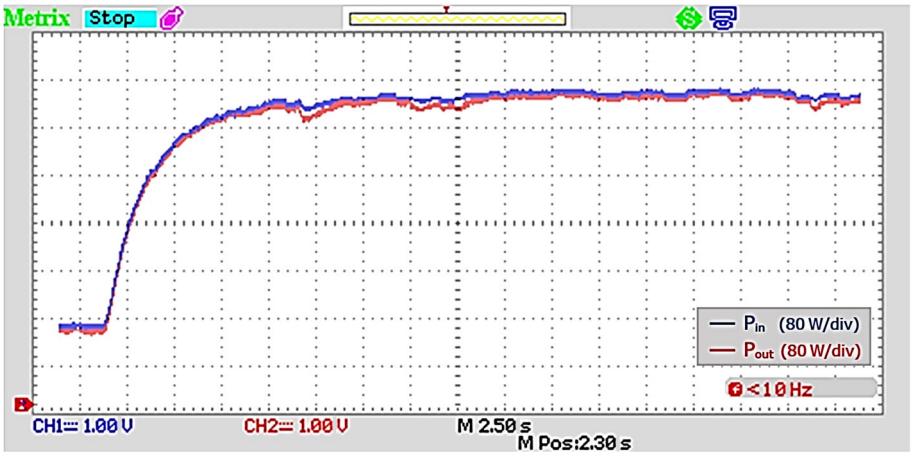

FIGURE 16 Input and output power of the DC-DC Buck converter when using conventional PI in the increasing wind speed condition.

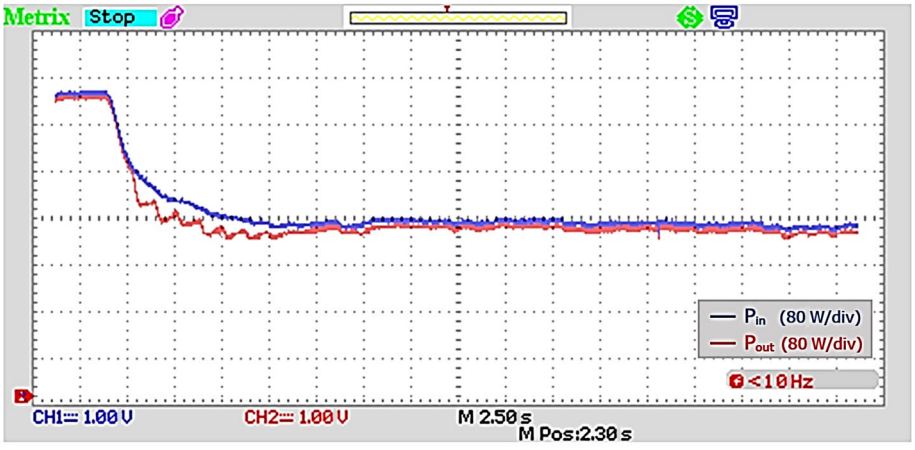

FIGURE 17 Input and output power of the DC-DC Buck converter when using conventional PI in the decreasing wind speed condition.

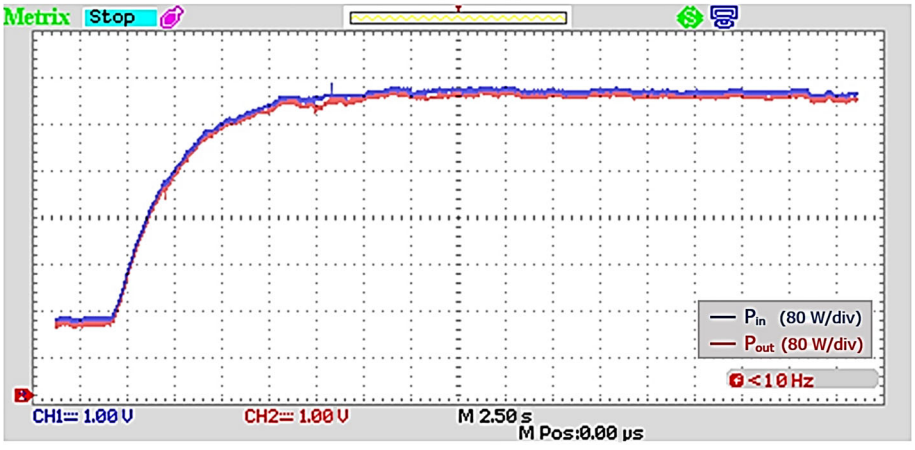

FIGURE 18 Input and output power of the DC-DC Buck converter when using nonlinear PI in the increasing wind speed condition.

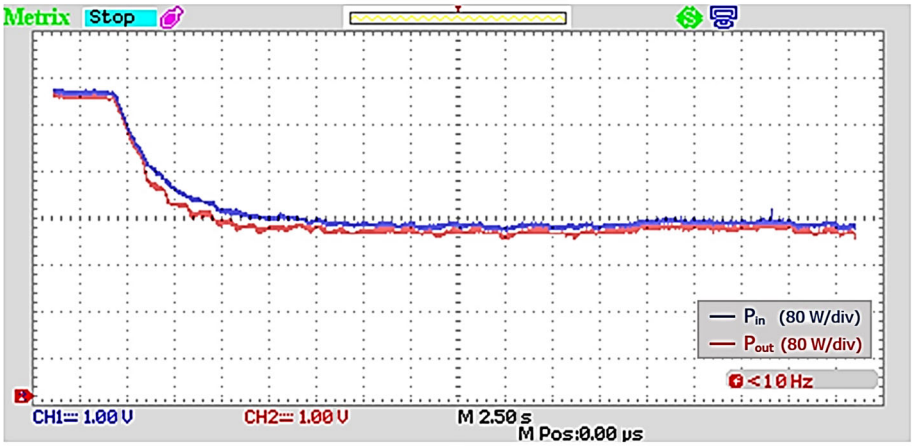

FIGURE 19 Input and output power of the DC-DC Buck converter when using nonlinear PI in the decreasing wind speed condition.

According to the presented results, it is noted that when using the NLPI, the input and output powers of the DC-DC Buck converter present lower oscillations when compared with the use of the CPI, and in the decreasing wind speed condition, the MPPT has faster convergence to the steady-state regime when using the NLPI.

5 | CONCLUSION

The paper presents a hardware realization and implementation of a WTE that succeeds in having the same static and dynamic behaviors as an actual WT. In the hardware realization, the prototype of the standalone wind energy conversion system emulator (WECSE) was developed with a separately excited DC motor to simulate the WT by providing the required speed and torque for power generation using a directly driven WRSG. The NLPI controller is used to control the DC motor torque for an estimated current reference through a chopper driven by a dSPACE (1104) controller board through MATLAB/Simulink. The experimental results show that the control and emulation performances of the NLPI controller are better compared to those obtained by the conventional one. Also, the test bench of the WECS has been tested using a modified drift-free P&O MPPT algorithm. The experimental results proved that when using the NLPI, the input and output powers of the DC-DC Buck converter present lower fluctuations and faster convergence to the maximum power point in the case of both an increase and a decrease in wind speed.

Future activities associated with this work propose the study for possible modifications in the experimental bench to minimize the problem of motor degaussing direct current for low rotations, as well as the replacement of the direct current motor with a generator doubly powered induction connected to the mains for the purpose to implement a control algorithm for the maximization of the power generated by the wind through the pitch angle. Furthermore, the hybridization of fuzzy logic with nonlinear PI control is the objective of a future research axis for this work.

ACKNOWLEDGMENTS

This work was carried out as part of a collaboration between Laboratoire de recherche: Commande, Analyse et Optimisation des Systémes Electro-Energétiques (CAOSEE), Université Tahri Mohamed de Bechar Algeria, Groupe de Recherche en Electronique de Puissance et Commande Industrielle (GRÉPCI), École de Téchnologie Supérieure (ÉTS), Montréal, Québec, Canada and Centre de Recherche de gestion énergétique intelligente des systèmes industriels et dans les bâtiments (CR2ie).Cégep de Sept-Îles, Québec, Canada.

ORCID

Abdeldjebar Hazzab https://orcid.org/0000-0001-5236-6619

REFERENCES

1. Ackermann T. *Wind Power in Power Systems. Wiley Online Library*; 2005.

2. Sewwandi K, Senarathna T, Lakshika K, et al. Wind turbine emulator for a microgrid. Paper presented at: 2017 Innovations in Power and Advanced Computing Technologies (i-PACT); April 21–22, 2017; Vellore, India. doi:10.1109/ipact.2017.8244901
3. De Oliveira J, Andreoli A. Wind turbine emulator: a tool for experimental and computational study. *IEEE Latin Am Trans*. 2021;19(11):1832-1839. doi:10.1109/TLA.2021.9475616
4. GWEC. *Global Wind Energy Outlook 2020*. GWEC; 2021. http://www.gwec.net
5. Castelló J, Espí JM, García-Gil R. Development details and performance assessment of a wind turbine emulator. *Renew Energy*. 2016;86:848-857. doi:10.1016/j.renene.2015.09.010
6. Soltoski J, Santos dP, Font C. Development of a small scale wind turbine emulator work bench. Paper presented at: 2016 12th IEEE International Conference on Industry Applications (INDUSCON); November 20–23, 2016; Curitiba, Brazil. doi:10.1109/INDUSCON39439.2016
7. Moussa I, Bouallegue A, Khedher A. Design and implementation of constant wind speed turbine emulator using Matlab/simulink and FPGA. Paper presented at: 2014 9th International Conference on Ecological Vehicles and Renewable Energies (EVER); March 25–27, 2014; Monte-Carlo, Monaco. doi:10.1109/INDUSCON39439.2016
8. Soliman M, Hasanien H, Azazi H, El-Kholy E, Mahmoud S. An adaptive fuzzy logic control strategy for performance enhancement of a grid-connected PMSG-based wind turbine. *IEEE Trans Ind Inform*. 2018;15(6):3163-3173. doi:10.1109/tii.2018.2875922
9. Yaylacı E. Discrete-time integral terminal sliding mode based maximum power point controller for the PMSG-based wind energy system. *IET Power Electron*. 2019;12(14):3688-3696. doi:10.1049/iet‐pel.2019.0106
10. Soliman M, Hasanien H, Azazi H, El-Kholy E, Mahmoud S. Hybrid ANFIS-GA-based control scheme for performance enhancement of a grid-connected wind generator. *IET Renew Power Gener*. 2018;12(7):832-843. doi:10.1049/iet‐rpg.2017.0576
11. Ghosh S, Isbeih Y, Bhattarai R, El Moursi M, El-Saadany E, Kamalasadan S. A dynamic coordination control architecture for reactive power capability enhancement of the DFIG-based wind power generation. *IEEE Trans on Power Syst*. 2020;35(4):3051-3064. doi:10.1109/tpwrs.2020.2968483
12. Yang RH, Jin JX. Unified power quality conditioner with advanced dual control for performance improvement of DFIG-based wind farm. *IEEE Trans on Sustain Energy*. 2020;12(1):116-126. doi:10.1109/tste.2020.2985161
13. Satpathy AS, Kastha D, Kishore N. Vienna rectifier fed squirrel cage induction generator based stand-alone wind energy conversion system. *IEEE Trans Power Electron*. 2021;36:10186-10198. doi:10.1109/TPEL.2021.3062694
14. Górski DA, Iwański G. Asynchronous grid connection of a cage induction generator excited by a power electronic converter. *IEEE Trans Energy Conv*. 2020;36(1):63-70. doi:10.1109/tec.2020.3011546
15. Hosseinabadi P, Pota H, Mekhilef S, Schwartz H. Fixed-time observer-based control of DFIG-based wind energy conversion systems for maximum power extraction. *Int J Electric Power Energy Syst*. 2023;146:108741. doi:10.1016/j.ijepes.2022.108741
16. Thapa KB, Jayasawal K. Pitch control scheme for rapid active power control of a PMSG-based wind power plant. *IEEE Trans Ind Appl*. 2020;56(6):6756-6766. doi:10.1109/tia.2020.3015169
17. Khodabakhsh J, Mohammadi E, Moschopoulos G. PMSG-based wind energy conversion systems integration into DC microgrids with a novel compact converter. *IEEE Access*. 2020;8:83583-83595. doi:10.1109/access.2020.2991668
18. Gouabi H, Hazzab A, Habbab M, Rezkallah M, Ambrish C. Experimental implementation of a novel scheduling algorithm for adaptive and modified P&O MPPT controller using fuzzy logic for WECS. *Int J Adapt Control Signal Process*. 2021;35(9):1732-1753. doi:10.1002/acs.3288
19. Suh Y, Lipo T. Field excitation scheme using a machine-side 4-leg converter in MW-range WRSG wind turbine systems. Paper presented at: 2017 IEEE Energy Conversion Congress and Exposition (ECCE); October 1–5 2017; Cincinnati, Ohio. doi:10.1109/ECCE.2017.8096598
20. Jahanpour-Dehkordi M, Vaez-Zadeh S, Mohammadi J. Development of a combined control system to improve the performance of a PMSG-based wind energy conversion system under normal and grid fault conditions. *IEEE Trans Energy Conv*. 2019;34(3):1287-1295. doi:10.1109/tec.2019.2912080
21. Moussa I, Bouallegue A, Khedher A. New wind turbine emulator based on DC machine: hardware implementation using FPGA board for an open-loop operation. *IET Circ Dev Syst*. 2019;13(6):896-902. doi:10.1049/iet‐cds.2018.5530
22. Chen P, Hu K, Lin Y, Liaw C. Development of a prime mover emulator using a permanent-magnet synchronous motor drive. *IEEE Trans Power Electron*. 2017;33(7):6114-6125. doi:10.1109/tpel.2017.2747221
23. Nair R, Narayanan G. Emulation of wind turbine system using vector controlled induction motor drive. *IEEE Trans on Ind Appl*. 2020;56(4):4124-4133. doi:10.1109/tia.2020.2987993
24. Hussain J, Mishra MK. Adaptive maximum power point tracking control algorithm for wind energy conversion systems. *IEEE Trans Energy Conv*. 2016;31(2):697-705. doi:10.1109/tec.2016.2520460
25. Llano DX, McMahon RA. Control techniques with system efficiency comparison for microwind turbines. *IEEE Trans Sustain Energy*. 2017;8(4):1609-1617. doi:10.1109/tste.2017.2698024
26. Su Y, Sun D, Duan B. Design of an enhanced nonlinear PID controller. *Mechatronics*. 2005;15(8):1005-1024. doi:10.1016/j.mechatronics.2005.03.003
27. Mokhtari F, Sicard P, Hazzab A. Decentralized nonlinear control strategies for disturbance rejection in winding systems. Paper presented at: 2011 IEEE International Electric Machines & Drives Conference (IEMDC); 2011; Niagara Falls, ON:230-235. doi:10.1109/IEMDC.2011.5994851
28. Haq IU, Khan Q, Khan I, Akmeliawati R, Nisar KS, Khan I. Maximum power extraction strategy for variable speed wind turbine system via neuro-adaptive generalized global sliding mode controller. *IEEE Access*. 2020;8:128536-128547. doi:10.1109/ACCESS.2020.2966053

29. Soliman MA, Hasanien HM, Al-Durra A, Debouza M. High performance frequency converter controlled variable-speed wind generator using linear-quadratic regulator controller. *IEEE Trans Ind Appl*. 2020;56(5):5489-5498. doi:10.1109/IAS.2019.8912454
30. Guo Y, Mohamed MEA. Speed control of direct current motor using ANFIS based hybrid PID configuration controller. *IEEE Access*. 2020;8:125638-125647. doi:10.1109/access.2020.3007615
31. Han J. From PID to active disturbance rejection control. *IEEE Trans Ind Electron*. 2009;56(3):900-906. doi:10.1109/tie.2008.2011621
32. Mishra J, Pattnaik M, Samanta S. Drift-free perturb and observe MPPT algorithm with improved performance for SEIG-based stand-alone wind energy generation system. *IEEE Trans Power Electron*. 2019;35(6):5842-5849. doi:10.1109/tpel.2019.2952324

How to cite this article: Hazzab A, Gouabi H, Habbab M, Rezkallah M, Ibrahim H, Chandra A. Wind turbine emulator control improvement using nonlinear PI controller for wind energy conversion system: Design and real-time implementation. *Int J Adapt Control Signal Process*. 2023;1-15. doi: 10.1002/acs.3566